

MINISTRY OF EDUCATION AND TRAINING MINISTRY OF CONSTRUCTION

UNIVERSITY OF TRANSPORT TECHNOLOGY

TRAN QUANG MINH

**NONLINEAR STABILITY AND DYNAMIC
ANALYSIS OF NANOCOMPOSITE PLATES AND
SHELLS WITH STIFFENERS IN CONSTRUCTION
STRUCTURES**

Major: Special Construction Engineering

Code : 9580206

SUMMARY OF DOCTORAL THESIS

HANOI – 2025

This work is completed at: University of Transport Technology

Scientific Supervisors:

- 1. Assoc. Prof. Dr. Vu Hoai Nam**
- 2. Assoc. Prof. Dr. Dang Thuy Dong**

Reviewer:

Reviewer:

Reviewer:

The thesis is defended before the University Council for Doctoral Thesis, meeting at the University of Transport Technology
at, date month year

This thesis can be found at:

- National Library of Vietnam
- Library of University of Transport Technology

INTRODUCTION

Nonlinear stability and dynamic analysis are important issues in structural mechanics, especially with advanced composite materials that can withstand large deformations. The nanocomposites with outstanding electro-thermo-mechanical properties promise to bring a turning point to engineering, requiring the expansion of the working range of structures in the large deflection state and with complex anisotropic properties. Today, the nanocomposites include FG-CNTRC, FG-GRC and FG-GPLRC, which are considered to have great potential in applications. To increase the load-bearing capacity of structures, stiffener design is an important solution that needs to be studied. The thesis focuses on the nonlinear analysis of stability and dynamics of stiffened nanocomposite plates and shells to meet modern design requirements. Therefore, this thesis researches "Nonlinear analysis of stability and dynamic of nanocomposite plates and shells with stiffeners in construction structures".

Research objectives of the thesis

1. Propose stiffener options and establish solutions for FG-GPLRC, and FG-GPLRC porous cored circular plates and spherical shells.
2. Propose stiffener options and establish solutions for complex curved panels, made of FG-CNTRC and FG-GRC with orthogonal stiffeners.
3. Propose stiffener options and establish solutions for FG-GPLRC and porous FG-GPLRC cylindrical shells with orthogonal and spiral stiffeners.
4. Analyze the nonlinear stability and dynamic behavior of structures and provide comments for the design calculation of construction structures.

Subject and scope of the thesis research

Research object: Common plate and shell structures in construction structures, such as: Panel, circular plate, spherical, and cylindrical shell.

Research scope: Nonlinear stability and dynamics problems.

Research Methodology

Analytical and semi-analytical approach.

Structure of the thesis

Includes introduction, 4 chapters, conclusion, list of author's scientific works and references.

Chapter 1. OVERVIEW OF THE RESEARCH PROBLEM

1.1. Types of materials with variable mechanical properties

1.1.2. Functionally graded Carbon nanotube reinforced composite

Carbon nanotubes (CNTs) with high tensile strength and excellent electrical and thermal conductivity, are the ideal choice for applications that require a material that is both strong and lightweight. Functionally graded Carbon nanotube reinforced composite (FG-CNTRC) combines an isotropic matrix material and continuously distributed CNTs, optimizing the mechanical properties and load-bearing capacity in plates and shells. Two popular models for determining the effective thermo-mechanical properties of FG-CNTRC are the Mori-Tanaka model and the rule of mixtures, which effectively support the analysis and design of load-bearing structures in harsh conditions.

1.1.3. Functionally graded Graphene reinforced composite

Graphene is a two-dimensional carbon material with outstanding mechanical, thermal and electrical properties, such as 100 times the strength of steel and 10 times the thermal conductivity of copper, making it an ideal choice for reinforcing matrix materials. Graphene-reinforced composites such as FG-GPLRC, FG-GRC and FG-GRMMC allow for optimization of mechanical properties by distributing the graphene volume fraction smoothly or piecewise in the structure. Research and application of these materials are expanding in many fields such as construction, aerospace and electronics, to enhance the strength, heat resistance and weight of structures.

1.1.4. Potential application of Nanocomposite and Nanocomposite plates and shells in construction engineering

1.1.4.1. Potential applications of Nanocomposites

Advanced composite materials such as FG-CNTRC, FG-GRC and FG-GPLRC are attracting attention in the construction industry due to their ability to increase durability, reduce weight, improve fire resistance and self-healing properties of structures. The application of these materials not only helps extend the life and reduce maintenance costs for buildings, but also opens up great economic and environmental potential, becoming an inevitable trend in the future.

1.1.4.2. Potential applications of Nanocomposite plates and shells

Nanocomposites with their lightweight, durable and superior corrosion resistance are being widely used in construction components such as floor slabs, roof shells, bridges and high-rise buildings, helping to increase durability and reduce maintenance costs. However, high production costs are currently a major obstacle to widespread use, but in the future, nanocomposites have the potential to replace traditional materials, contributing to the sustainable and safe development of the construction.

1.2. Research situation at home and abroad

1.2.1. Studies on FGM plates and shells

Many international authors have studied FGM plates and shells such as Shen [124, 129, 130], Sofiyev et al. [143-145], Hong [60], Liu et al. [78], Elmhaia et al. [48], Javani et al. [64], He et al. [55], and Vietnamese authors [2, 4, 5, 13-20, 32, 33, 38-40, 44-47, 88-91, 93, 108, 111].

1.2.2. Studies on FG-CNTRC plates and shells

Shen et al. [126-128, 131], Kiani [66, 67], Alibeigloo and Liew [7], Lei et al. [77], Zeighami and Jafari [170], Salehipour et al. [54], Khayat et al. [72], Raissi [119], Mehri et al. [83], Zhao et al. [171], Sobhani and Safaei [142], Vietnamese authors [3, 6, 34-36, 41-43, 56-58, 84, 92, 94, 150-154].

1.2.3. Studies on FG-GPLRC plates and shells

Gholami and Ansari [51], Yang et al. [166], Chen et al. [26], Song et al. [147], Namazinia et al. [105], Bidzard et al. [21], Chen and Li [25], Barati and Zenkour [11], Wang et al. [158, 159], Hu et al. [61], Yang et al. [165], Yang et al. [167], Yasin et al. [168], Phuong et al. [114], Ly et al. [81], Nam et al. [100, 102].

1.2.4. Studies on the FG-GRC and FG-GRMMC plates and shells

Shen et al. [132-135, 137, 138], Kiani et al. [68-71], Authors of University of Transport Technology [1, 29, 30, 87, 95-98, 109, 110, 113, 115-117].

1.3. Results achieved domestically and internationally

1- Relatively comprehensive analysis of linear and nonlinear static stability of FG-CNTRC, FG-GRC and FG-GPLRC plates and shells using different methods, and different plate and shell theories.

2- Relatively comprehensive investigation of dynamic stability, linear and nonlinear vibrations of some FG-CNTRC, FG-GRC and FG-GPLRC structures under different loading conditions, using different methods.

3- Types of stiffeners such as spiderweb stiffener (with circular plates and spherical shells), spiral stiffener with cylindrical shells have not been focused on previous works. Complex curved panels such as sine, parabolic panels with stiffeners have not been researched.

1.4. Conclusion of Chapter 1 and problems that need further research

1- Establish improved stiffener effect leveling techniques for FG-GPLRC stiffeners with spider and spiral stiffener designs.

2- Study on stability and nonlinear dynamics of circular plate and spherical shell FG-GLRC with spiderweb stiffeners subjected to mechanical and thermal loads.

3- Study on stability and nonlinear dynamics of cylindrical panel, parabolic panel and sine panel FG-CNTRC and FG-GRC with stiffeners FG-CNTRC and FG-GRC respectively subjected to different types of loads.

4- Study on the stability and postbuckling of static nonlinear stability of FG-GPLRC and porous FG-GPLRC cylindrical shells with orthogonal and spiral stiffeners.

Chapter 2. STABILITY AND NONLINEAR DYNAMICS OF FG-GPLRC CIRCULAR PLATE AND SPHERE STIFFENESS BY SPIDER WEB TENION SYSTEM

This chapter proposes an analytical algorithm to analyze the postbuckling behavior of the proposed spiderweb stiffened circular plate and spherical shell. This algorithm extends the Lekhnitskii's smeared stiffener technique and uses the energy method. The main points in this chapter include the design of the GPL distribution law in the stiffeners and circular plate/spherical shell, the spatial design of the spiderweb stiffeners, and the investigation of the influence of parameters on the stability and nonlinear dynamic behavior of the structure.

2.1. Structural and material models

2.1.1. Structural model

The spherical shell has thickness h and radius R_c and base radius a_{ou} placed on a nonlinear elastic foundation as shown in Figure 2.1.

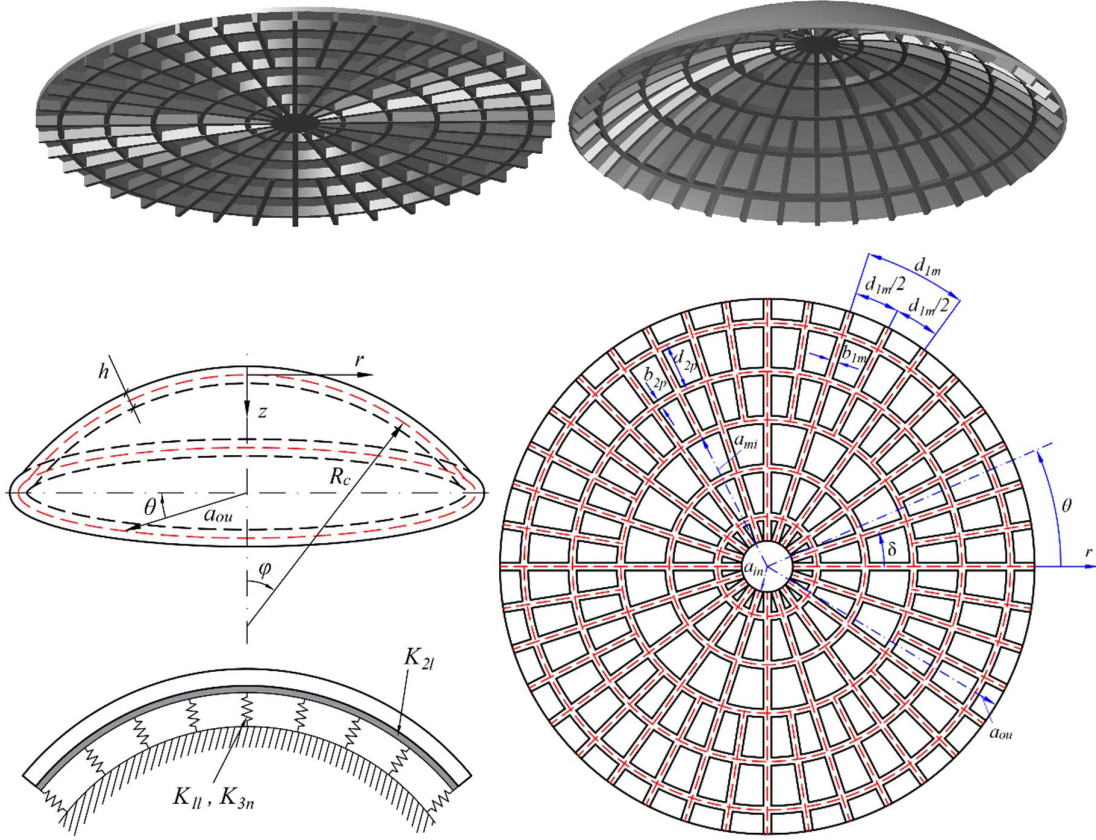


Figure 2.2. Coordinate system and model of the spherical shells and circular plate stiffened by three-region spiderweb stiffeners

2.1.2. Material model

2.1.2.1. FG-GPLRC spherical shell and circular plate stiffened by FG-GPLRC spiderweb stiffeners and with piezoelectric layer

Five GPL distribution types (Fig. 2.3) according to the thickness of the shell ($-h/2 + h_v \leq z \leq h/2$) are used for GPL volume fractions, as

$$\Lambda_G^{sh} = \begin{cases} \Lambda_G & \text{UD-GPLRC,} \\ \left[\frac{|4z - 2h_v|}{(-h_v + h)} \right] \Lambda_G & \text{X-GPLRC,} \\ \left[2 - \frac{|4z - 2h_v|}{(-h_v + h)} \right] \Lambda_G & \text{O-GPLRC,} \\ \left[\frac{-2z + h}{(h - h_v)} \right] \Lambda_G & \text{V-GPLRC,} \\ \left[\frac{-2h_v + h + 2z}{(h - h_v)} \right] \Lambda_G & \text{A-GPLRC,} \end{cases} \quad (2.1)$$

and for stiffeners ($h/2 \leq z \leq h/2 + h_{st}$)

$$\Lambda_G^{st} = \begin{cases} \Lambda_G & \text{UD-GPLRC,} \\ \left[\frac{(-4z + 2h)}{h_{st}} + 2 \right] \Lambda_G & \text{X-GPLRC,} \\ \left[2 - \frac{(-2h + 4z)}{h_{st}} - 2 \right] \Lambda_G & \text{O-GPLRC,} \\ \left[\frac{(-2z + h)}{h_{st}} + 2 \right] \Lambda_G & \text{V-GPLRC,} \\ \left[\frac{(-h + 2z)}{h_{st}} \right] \Lambda_G & \text{A-GPLRC,} \end{cases} \quad (2.2)$$

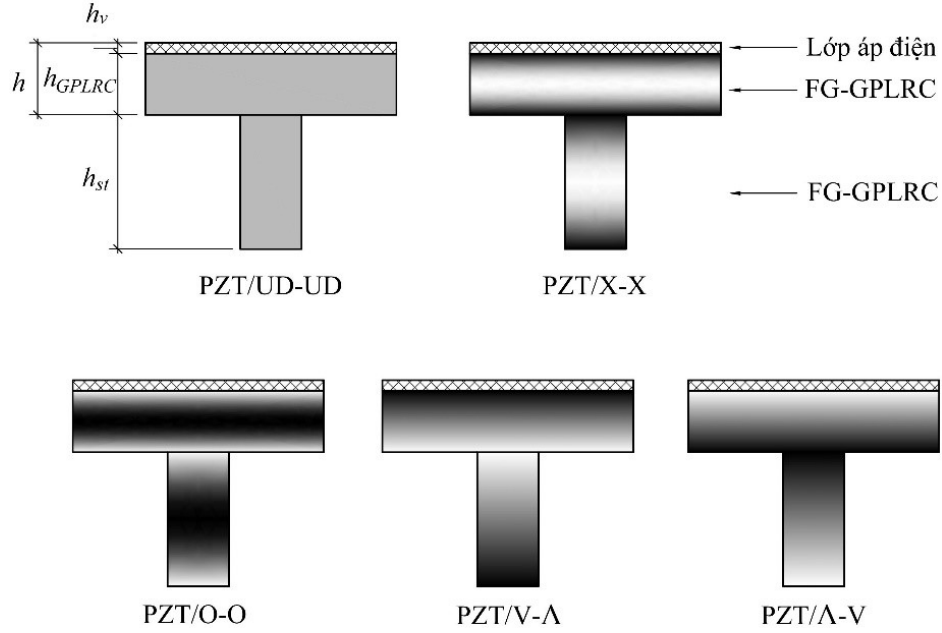


Fig. 2.3. Types of GPL distribution of the spherical shell and stiffeners
2.1.2.2. *FG-GPLRC porous cored spiderweb stiffened FG-GPLRC circular plates and spherical shells*

The five laws of GPL mass distribution of the upper layer are as follows ($-h/2 \leq z \leq -h_{cc}/2$)

$$\Lambda_G^T = \begin{cases} \Lambda_G & \text{UD-GPLRC,} \\ \left[\frac{(2h_{cc} + 2h + 8z)}{(-h_{cc} + h)} \right] \Lambda_G & \text{X-GPLRC,} \\ \left[2 - \frac{(2h_{cc} + 2h + 8z)}{(-h_{cc} + h)} \right] \Lambda_G & \text{O-GPLRC,} \\ \left[\frac{(2h_{cc} + 4z)}{(h_{cc} - h)} \right] \Lambda_G & \text{V-GPLRC,} \\ \left[\frac{-(2h + 4z)}{(h_{cc} - h)} \right] \Lambda_G & \text{A-GPLRC,} \end{cases} \quad (2.8)$$

The GPL distribution rules of the lower layer and spiderweb stiffeners are designed according to the corresponding laws.

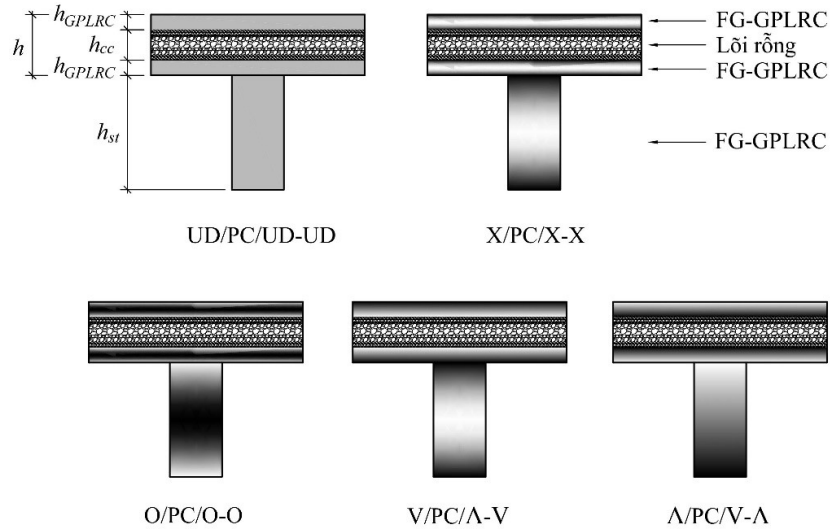


Fig. 2.4. Design of distribution rules of shell skin layers and stiffeners

2.2. Basic equations and solution methods

2.2.1. Basic formulas and equations

The expressions for extension and moment are derived as

$$\begin{aligned}
 N_r &= J_{11} \bar{\varepsilon}_r + J_{12} \bar{\varepsilon}_\theta - F_{11} w_{,rr} - F_{12} \frac{w_{,r}}{r} - \phi_{1r}^T \Delta T - \phi_{1r}^v V_e, \\
 N_\theta &= J_{12} \bar{\varepsilon}_r + J_{22} \bar{\varepsilon}_\theta - F_{12} w_{,rr} - F_{22} \frac{w_{,r}}{r} - \phi_{1\theta}^T \Delta T - \phi_{1\theta}^v V_e, \\
 M_r &= F_{11} \bar{\varepsilon}_r + F_{12} \bar{\varepsilon}_\theta - P_{11} w_{,rr} - P_{12} \frac{w_{,r}}{r} - \phi_{2r}^T \Delta T - \phi_{2r}^v V_e, \\
 M_\theta &= F_{12} \bar{\varepsilon}_r + F_{22} \bar{\varepsilon}_\theta - P_{12} w_{,rr} - P_{22} \frac{w_{,r}}{r} - \phi_{2\theta}^T \Delta T - \phi_{2\theta}^v V_e,
 \end{aligned} \tag{2.22}$$

The strain energy with thermo-mechanical components, work done by external pressure, foundation interactions, and kinetic energy are as

$$\begin{aligned}
 \Phi_{\text{int}} &= \pi \int_{\Gamma} \int_0^{a_{in}} \left\{ \sigma_r \varepsilon_r + \sigma_\theta \varepsilon_\theta - (\sigma_r + \sigma_\theta) [\bar{\alpha}(z) \Delta T + (d_v/h_v) V_e] \right\} r dr dz \\
 &+ \pi \int_{\Gamma} \int_{a_{in}}^{a_{mi}} \left\{ \sigma_r \varepsilon_r + \sigma_\theta \varepsilon_\theta - (\sigma_r + \sigma_\theta) [\bar{\alpha}(z) \Delta T + (d_v/h_v) V_e] \right\} r dr dz \tag{2.23} \\
 &+ \pi \int_{\Gamma} \int_{a_{mi}}^{a_{ou}} \left\{ \sigma_r \varepsilon_r + \sigma_\theta \varepsilon_\theta - (\sigma_r + \sigma_\theta) [\bar{\alpha}(z) \Delta T + (d_v/h_v) V_e] \right\} r dr dz
 \end{aligned}$$

$$\Phi_{\text{ext}} = 2\pi \int_0^{a_{ou}} qwr dr - \pi \int_0^{a_{ou}} \left\{ \left[\frac{K_{3n} w^3}{2} - K_{2l} \left(w_{,rr} + \frac{w_{,r}}{r} \right) + K_{1l} w \right] w \right\} r dr \tag{2.24}$$

$$\Phi_T = \pi \int_{\Gamma} \int_0^{a_{in}} \bar{\rho}(z) \bar{w}_t^2 r dr dz + \pi \int_{\Gamma} \int_{a_{in}}^{a_{mi}} \bar{\rho}(z) \bar{w}_t^2 r dr dz + \pi \int_{\Gamma} \int_{a_{mi}}^{a_{ou}} \bar{\rho}(z) \bar{w}_t^2 r dr dz, \quad (2.25)$$

The Lagrange function is obtained as

$$\Phi = \Phi_T - \Phi_{int} + \Phi_{ext}. \quad (2.26)$$

Based on boundary conditions (2.27), the solutions are chosen [13]

$$u = U \frac{r a_{ou} - r^2}{a_{ou}^2}, \quad w = W \frac{(a_{ou}^2 - r^2)^2}{a_{ou}^4}, \quad w^* = \lambda h \frac{(a_{ou}^2 - r^2)^2}{a_{ou}^4}. \quad (2.28)$$

The potential energy of the system is determined as follows

$$D = \pi \int_0^{a_{ou}} \kappa w_t^2 r dr \quad (2.29)$$

Euler–Lagrange equation combines Rayleigh dissipation function, is

$$\frac{d}{dt} \left(\frac{\partial \Phi}{\partial \dot{W}} \right) - \frac{\partial \Phi}{\partial W} + \frac{\partial D}{\partial \dot{W}} = 0, \quad \frac{d}{dt} \left(\frac{\partial \Phi}{\partial \dot{U}} \right) - \frac{\partial \Phi}{\partial U} = 0, \quad (2.30)$$

lead to

$$I_{11} U + I_{12} W + I_{13} W(W + 2\lambda h) + I_{14} \Delta T + I_{15} V_e = 0, \quad (2.31)$$

$$I_{12} U + I_{22} U(W + \lambda h) + I_{23} W(W + 4\lambda h/3) + I_{25} W^3 K_{3n} + I_{30} \Delta T \\ + I_{24} W(W + \lambda h)(W + 2\lambda h) + (I_{26} K_{1l} + I_{27} K_{2l} + I_{28}) W + I_{35} V_e \quad (2.32)$$

$$+ I_{29} \Delta T(W + \lambda h) + I_{34} V_e(W + \lambda h) + I_{31} q - I_{32} \ddot{W} - I_{33} \kappa \dot{W} = 0,$$

By solving Eq. (2.31), we obtain the amplitude expression U , then, substituting the obtained expression into Eq. (2.32), leads to

$$\left(I_{26} K_{1l} + I_{27} K_{2l} + I_{28} - \frac{I_{12}^2}{I_{11}} \right) W - \frac{I_{12} I_{22}}{I_{11}} W(W + \lambda h) + I_{25} W^3 K_{3n} \\ - \frac{I_{12} I_{13}}{I_{11}} W(W + 2\lambda h) + \left(I_{24} - \frac{I_{13} I_{22}}{I_{11}} \right) W(W + \lambda h)(W + 2\lambda h) + I_{31} q \\ + I_{23} W \left(W + \frac{4}{3} \lambda h \right) + \left(I_{29} - \frac{I_{14} I_{22}}{I_{11}} \right) \Delta T(W + \lambda h) + \left(I_{30} - \frac{I_{12} I_{14}}{I_{11}} \right) \Delta T \\ + \left(I_{34} - \frac{I_{15} I_{22}}{I_{11}} \right) V_e(W + \lambda h) + \left(I_{35} - \frac{I_{12} I_{15}}{I_{11}} \right) V_e - I_{32} \ddot{W} - I_{33} \kappa \dot{W} = 0, \quad (2.33)$$

The Runge-Kutta method is applied to solve Eq. (2.33). The functions $q = \vartheta t$ and $\Delta T = \eta t$ are chosen for the external pressure and thermal load.

2.3. Numerical results and discussion

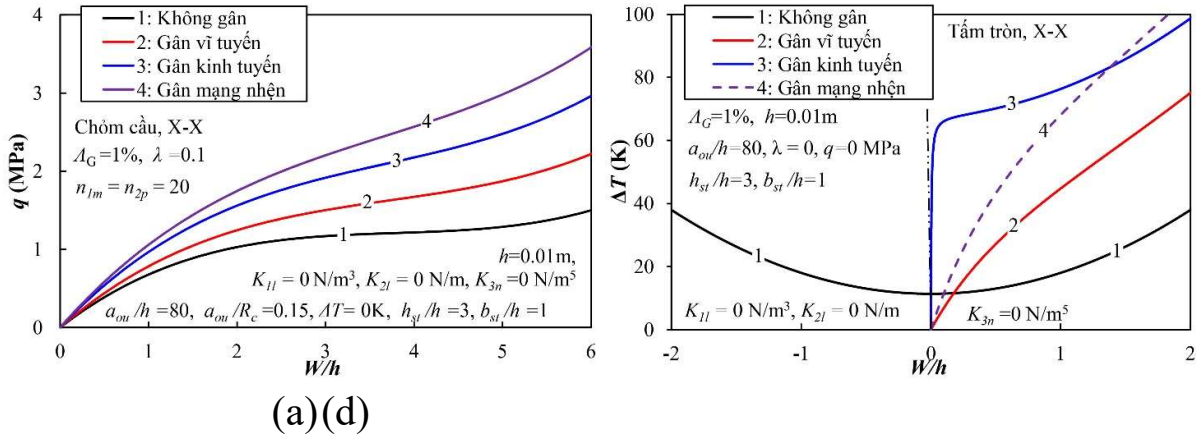


Fig. 2.6. Effect of stiffeners and type of stiffeners on the postbuckling behavior of FG-GPLRC spherical shell/circular plate

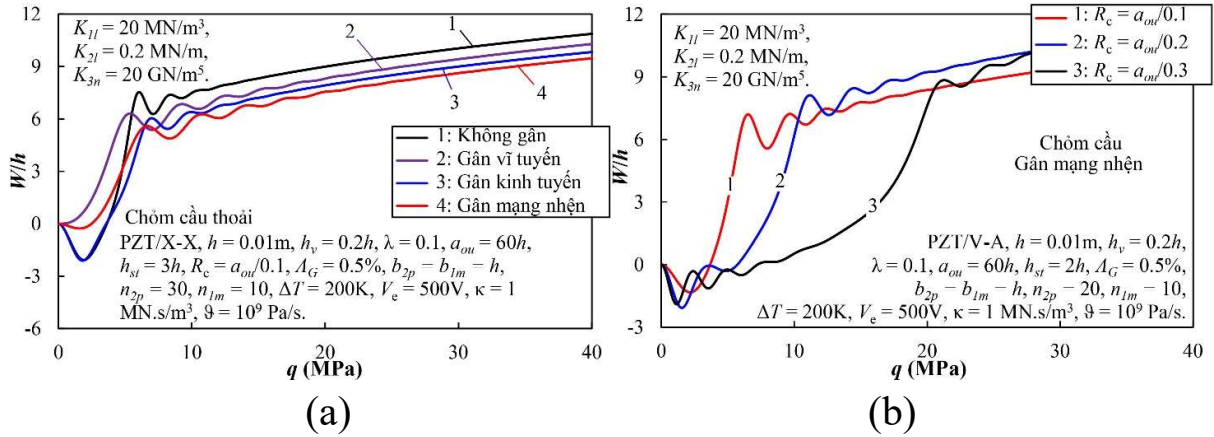


Fig. 2.13. Dynamic response to buckling of three-region stiffened circular plate and spherical shell under external pressure

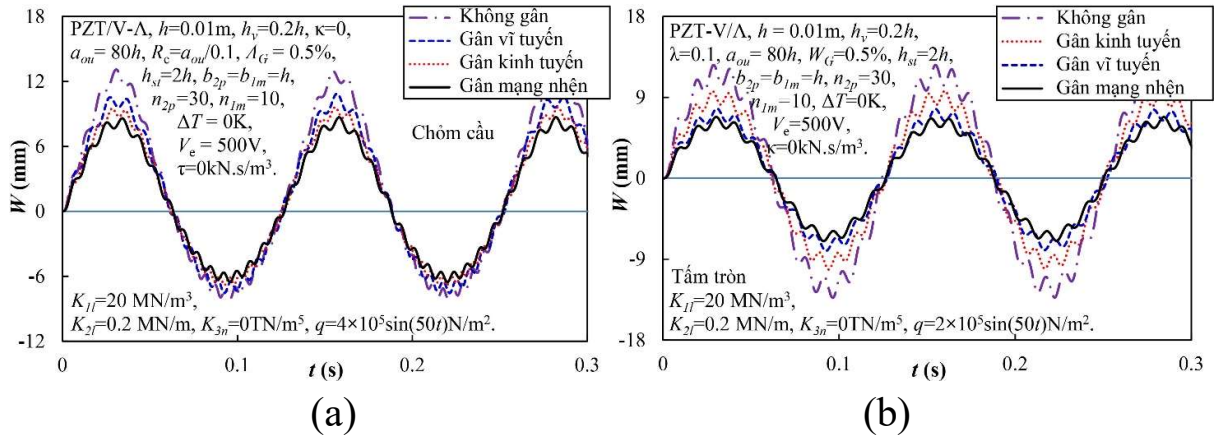


Fig. 2.21. Amplitude-time curves of FG-GPLRC circular plates and spherical shells with different stiffener types and material parameters

2.4. Conclusion of Chapter 2

From the numerical examples, some notable observations are as follows:

- The bifurcation phenomenon was only observed for unstiffened FG-GPLRC circular plates under thermal loading.
- The stiffeners increase the capacity of the spherical shells and circular plates, and reduce the snap-through buckling of the spherical shells.
- The influence of spiderweb stiffeners on the postbuckling behavior is most evident in the thermal postbuckling curve of the circular plates.
- Spiderweb stiffeners show outstanding effects in improving natural frequency, reducing amplitude and increasing dynamic stability.
- The effects of geometric, material parameters, and foundation on the stability and dynamic behavior are evident in the numerical examples.

CHAPTER 3: NONLINEAR STABILITY AND DYNAMICS OF FG-CNTRC AND FG-GRC PANELS WITH COMPLEX CURVES AND ORTHOGONAL STIFFENERS

This chapter presents the nonlinear stability and dynamic of parabolic, sine and cylindrical panels made from FG-CNTRC and FG-GRC stiffened by FG-CNTRC and FG-GRC stiffeners respectively considering uniform temperature and piezoelectric layers.

3.1. Design of geometrical and material parameters of FG-CNTRC and FG-GRC cylindrical, parabolic, and sine panels

Consider cylindrical, parabolic and sine panels, resting on elastic foundation, under external pressure and axial loads as shown in Fig. 3.1. The geometric radii of the parabolic and the sine panel in the curved direction can be easily obtained from Eq. (3.1), as [1]

$$R_{PPs} = \frac{\left[16\delta^2(b-2y)^2 + b^4\right]^{3/2}}{8b^4\delta}, \quad R_{SPs} = \frac{\left[\pi^2\delta^2 \cos^2 \frac{\pi y}{b} + b^2\right]^{3/2}}{\pi^2 b \delta \sin \frac{\pi y}{b}}. \quad (3.2)$$

3.1.1. FG-CNTRC panel with FG-CNTRC stiffeners and piezoelectric layer

CNT distribution rules according to thickness $(-h/2 + h_v \leq z \leq h/2)$ expressed through homogeneous or linear functions, as follows

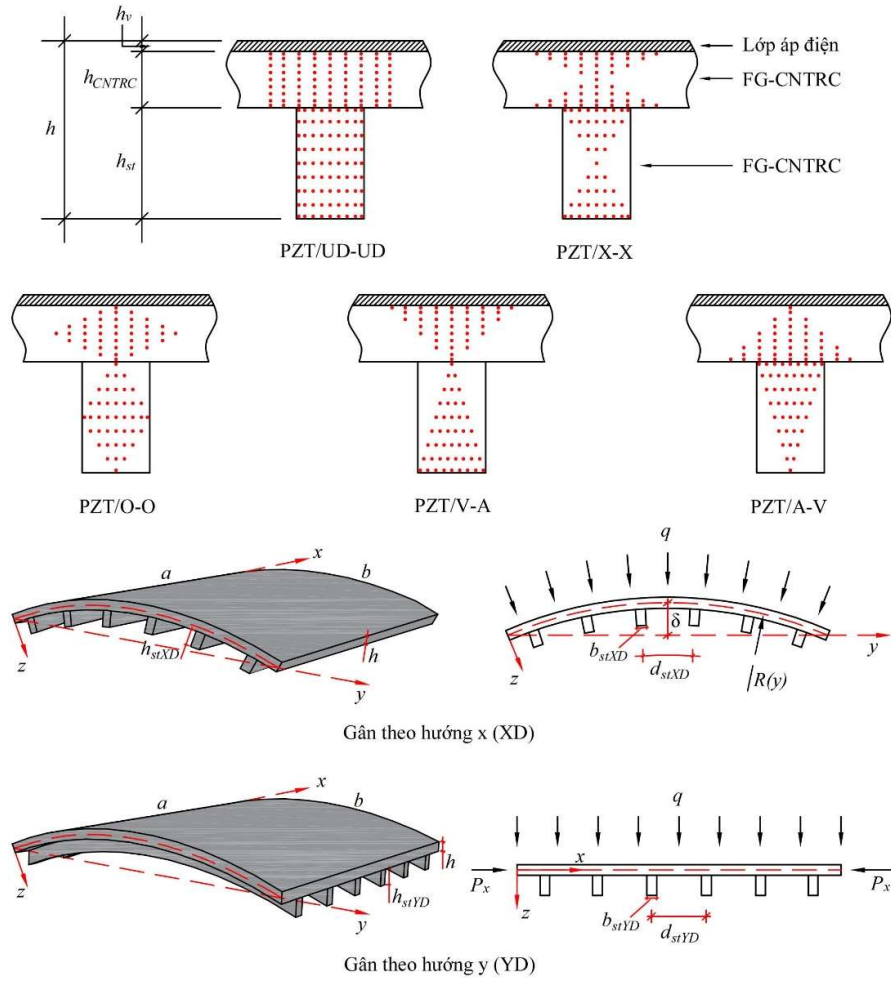


Fig. 3.1 . Design model and distribution model of CNTs for stiffened panels and piezoelectric layers

$$V_{CNT} = \begin{cases} V_{CNT}^* & \text{UD-CNTRC} \\ \left(\frac{4|z - h_v/2|}{h - h_v} \right) V_{CNT}^* & \text{X-CNTRC} \\ \left(2 - \frac{4|z - h_v/2|}{h - h_v} \right) V_{CNT}^* & \text{O-CNTRC} \\ \left(\frac{h - 2z}{h - h_v} \right) V_{CNT}^* & \text{V-CNTRC} \\ \left(\frac{2z + h - 2h_v}{h - h_v} \right) V_{CNT}^* & \text{A-CNTRC} \end{cases} \quad (3.3)$$

and for the stiffeners ($h/2 \leq z \leq h/2 + h_{st}$)

$$V_{CNT} = \begin{cases} V_{CNT}^* & \text{UD-CNTRC} \\ \left| \frac{2h-4z}{h_{st}} + 2 \right| V_{CNT}^* & \text{X-CNTRC} \\ \left(2 - \left| \frac{4z-2h}{h_{st}} - 2 \right| \right) V_{CNT}^* & \text{O-CNTRC} \\ \left(2 + \frac{h-2z}{h_{st}} \right) V_{CNT}^* & \text{V-CNTRC} \\ \frac{2z-h}{h_{st}} V_{CNT}^* & \text{A-CNTRC} \end{cases} \quad (3.4)$$

3.1.2. Model of FG-GRC panel with stiffeners on Pasternak foundation

The cylindrical, parabolic, sine panels and stiffeners are made from FG-GRC, with five graphene distribution types including UD, FG-X, FG-V, FG-A and FG-O, and three graphene arrangements including $(0)_{10T}$, $(0/90)_{5T}$ and $(0/90/0/90/0)_S$.

3.2 . Theoretical basis and improved smeared stiffener technique

Components of extension, moment, and higher order moment of the internal mechanical, thermal and electrical force components of the panel combined with the anisotropic smeared stiffener technique [1, 6] within the framework of HSDT, is obtained as follows

$$\begin{Bmatrix} N_x \\ N_y \\ N_{xy} \\ M_x \\ M_y \\ M_{xy} \\ T_x \\ T_y \\ T_{xy} \end{Bmatrix} = \begin{bmatrix} A_{11} & A_{12} & 0 & B_{11} & B_{12} & 0 & D_{11} & D_{12} & 0 \\ A_{12} & A_{22} & 0 & B_{12} & B_{22} & 0 & D_{12} & D_{22} & 0 \\ 0 & 0 & A_{66} & 0 & 0 & B_{66} & 0 & 0 & D_{66} \\ B_{11} & B_{12} & 0 & C_{11} & C_{12} & 0 & F_{11} & F_{12} & 0 \\ B_{12} & B_{22} & 0 & C_{12} & C_{22} & 0 & F_{12} & F_{22} & 0 \\ 0 & 0 & B_{66} & 0 & 0 & C_{66} & 0 & 0 & F_{66} \\ D_{11} & D_{12} & 0 & F_{11} & F_{12} & 0 & L_{11} & L_{12} & 0 \\ D_{12} & D_{22} & 0 & F_{12} & F_{22} & 0 & L_{12} & L_{22} & 0 \\ 0 & 0 & D_{66} & 0 & 0 & F_{66} & 0 & 0 & L_{66} \end{bmatrix} \times$$

$$\times \begin{bmatrix} \bar{\varepsilon}_x \\ \bar{\varepsilon}_y \\ \bar{\gamma}_{xy} \\ \phi_{x,x} \\ \phi_{y,y} \\ \phi_{y,x} + \phi_{x,y} \\ -\lambda(w_{,xx} + \phi_{x,x}) \\ -\lambda(w_{,yy} + \phi_{y,y}) \\ -\lambda(\phi_{y,x} + 2w_{,xy} + \phi_{x,y}) \end{bmatrix} - \begin{bmatrix} \Phi_{1x} \\ \Phi_{1y} \\ 0 \\ \Phi_{2x} \\ \Phi_{2y} \\ 0 \\ \Phi_{4x} \\ \Phi_{4y} \\ 0 \end{bmatrix}, \quad (3.10)$$

Combining the forces and moments (3.10) and the condition (3.16), the deformation compatibility equation (3.15) is re-represented as

$$\begin{aligned} \Theta \equiv & A_{22}^* \zeta_{,xxxx} + (A_{66}^* + 2A_{12}^*) \zeta_{,xxyy} + A_{11}^* \zeta_{,yyyy} + (B_{21}^* - \lambda C_{21}^*) \phi_{x,xxx} \\ & + (\lambda C_{66}^* - \lambda C_{11}^* + B_{11}^* - B_{66}^*) \phi_{x,xyy} + (\lambda C_{66}^* - \lambda C_{22}^* + B_{22}^* - B_{66}^*) \phi_{y,xyy} \\ & + (B_{12}^* - \lambda C_{12}^*) \phi_{y,yyy} - \lambda C_{21}^* w_{,xxxx} - \lambda (C_{11}^* + C_{22}^* - 2C_{66}^*) w_{,xxyy} - w_{,xy}^2 \\ & - \lambda C_{12}^* w_{,yyyy} + \frac{w_{,xx}}{R(y)} + w_{,xx} w_{,yy} + w_{,xx} w_{,yy}^* - 2w_{,xy} w_{,xy}^* + w_{,xx}^* w_{,yy} = 0. \end{aligned} \quad (3.17)$$

3.3 . Boundary conditions, stress function approximation and Euler-Lagrange equation

To satisfy the boundary conditions at the four edges, the solutions of the deflection, rotation and imperfect of the panel are chosen as

$$\begin{aligned} w &= W \sin \alpha x \sin \beta y, \quad w^* = \xi h \sin \alpha x \sin \beta y \\ \phi_x &= \Phi_x \cos \alpha x \sin \beta y, \quad \phi_y = \Phi_y \sin \alpha x \cos \beta y, \end{aligned} \quad (3.20)$$

Due to the complex curvature in the compatibility equation (3.17), it is not possible to determine the exact stress function form of the parabolic and sine panels. The stress function form is chosen as

$$\zeta = \zeta_1 \cos 2\alpha x + \zeta_2 \cos 2\beta y + \zeta_3 \sin \alpha x \sin \beta y + \frac{1}{2} N_{0y} x^2 + \frac{1}{2} N_{0x} y^2. \quad (3.21)$$

An approximate technique to determine the stress function form for parabolic and sine panels can be done as follows

$$\int_0^b \int_0^a \Theta \cos 2\alpha x \, dx dy = 0, \int_0^b \int_0^a \Theta \cos 2\beta y \, dx dy = 0, \int_0^b \int_0^a \Theta \sin \alpha x \sin \beta y \, dx dy = 0. \quad (3.22)$$

The strain energy, work done by the external force considering the interaction between the panel and the foundation is calculated as follows

$$\Phi_{in} = \frac{1}{2} \int_{-h/2}^{h/2} \int_0^b \int_0^a \left[\begin{aligned} &\sigma_x \left(\varepsilon_x - \alpha_{11} \Delta T - \frac{d_{31} V_e}{h_v} \right) \\ &+ \sigma_y \left(\varepsilon_y - \alpha_{22} \Delta T - \frac{d_{32} V_e}{h_v} \right) \\ &+ \sigma_{xy} (\gamma_{xy} - \alpha_{12} \Delta T) + \sigma_{xz} \gamma_{xz} + \sigma_{yz} \gamma_{yz} \end{aligned} \right] dx dy dz, \quad (3.25)$$

$$\Phi_{ext} = \int_0^b \int_0^a q w dx dy - \int_0^b \int_0^a \left\{ \frac{1}{2} w \left[K_1 w - K_2 (w_{,xx} + w_{,yy}) \right] \right\} dx dy$$

$$+ N_{0x} \int_0^b \int_0^a \left(\bar{\varepsilon}_x - \frac{w_{,x}^2}{2} - w_{,x} w_{,x}^* \right) dx dy, \quad (3.26)$$

Kinetic energy in z direction can be obtained as

$$\Phi_T = \frac{1}{2} \int_{-h/2}^{h/2} \int_0^b \int_0^a \rho \bar{w}_{,t}^2 dx dy dz. \quad (3.27)$$

The Lagrange function can be represented as

$$\Phi = \Phi_T - \Phi_{in} + \Phi_{ext}. \quad (3.28)$$

The potential energy of damping of the structure using the Rayleigh dissipation function can be expressed as

$$D = \frac{1}{2} \int_0^b \int_0^a \kappa \dot{w}^2 dx dy. \quad (3.29)$$

The Euler-Lagrange equations can be applied in combination with the Rayleigh dissipation function as follows

$$\frac{d}{dt} \left(\frac{\partial \Phi}{\partial \dot{W}} \right) - \frac{\partial \Phi}{\partial W} + \frac{\partial D}{\partial \dot{W}} = 0,$$

$$\frac{d}{dt} \left(\frac{\partial \Phi}{\partial \dot{\Phi}_x} \right) - \frac{\partial \Phi}{\partial \Phi_x} = 0, \quad \frac{d}{dt} \left(\frac{\partial \Phi}{\partial \dot{\Phi}_y} \right) - \frac{\partial \Phi}{\partial \Phi_y} = 0. \quad (3.30)$$

leads to

$$\begin{aligned} & \Psi_{11} W + \Phi_x \Psi_{12} + \Phi_y \Psi_{13} + \Phi_x \Psi_{14} (h\xi + W) + \Phi_y \Psi_{15} (h\xi + W) \\ & + \Psi_{16} W \left(W + \frac{4}{3} h\xi \right) + \Psi_{17} W (2h\xi + W) (h\xi + W) + \Psi_{18} N_{0x} \end{aligned} \quad (3.31)$$

$$\begin{aligned} & + \Psi_{19} N_{0x} (h\xi + W) + \Psi_{20} N_{0y} - \Psi_{22} q - \Psi_{23} + \Psi_{24} \ddot{W} + \Psi_{25} \kappa \dot{W} = 0, \\ & \Psi_{12} W + L_{22} \Phi_x + L_{23} \Phi_y \\ & + L_{24} W (2h\xi + W) + L_{25} N_{0x} + L_{26} N_{0y} - L_{27} = 0, \end{aligned} \quad (3.32)$$

$$\begin{aligned} & \Psi_{13} W + L_{23} \Phi_x \\ & + \Upsilon_{23} \Phi_y + \Upsilon_{24} W (2h\xi + W) + \Upsilon_{25} N_{0x} + \Upsilon_{26} N_{0y} - \Upsilon_{27} = 0, \end{aligned} \quad (3.33)$$

The motion equation is received as

$$\begin{aligned} & (\Xi_{12} + \vartheta \Xi_{19} \Lambda_{34}) (h\xi + W) + (\Xi_{13} + \vartheta \Xi_{19} \Lambda_{32}) W (h\xi + W) + \vartheta \Xi_{18} \Lambda_{34} \\ & - P_x h (\Xi_{17} + \vartheta \Xi_{19} \Lambda_{33}) (h\xi + W) + (\Xi_{14} + \vartheta \Xi_{18} \Lambda_{31}) W (2h\xi + W) \\ & - P_x h (\Xi_{16} + \vartheta \Xi_{18} \Lambda_{33}) + (\Xi_{11} + \vartheta \Xi_{18} \Lambda_{32}) W + \Xi_{20} + \Psi_{24} \ddot{W} + \Psi_{25} \kappa \dot{W} \\ & + \Psi_{16} W \left(W + \frac{4}{3} h\xi \right) + (\Xi_{15} + \vartheta \Xi_{19} \Lambda_{31}) W (2h\xi + W) (h\xi + W) = \Psi_{22} q \end{aligned} \quad (3.37)$$

Eq. (3.37) is solved using the fourth-order Runge-Kutta method to obtain the dynamic response of the panel. The dynamic critical buckling load is determined using the Budiansky-Roth criterion.

3.4. Numerical results and discussion

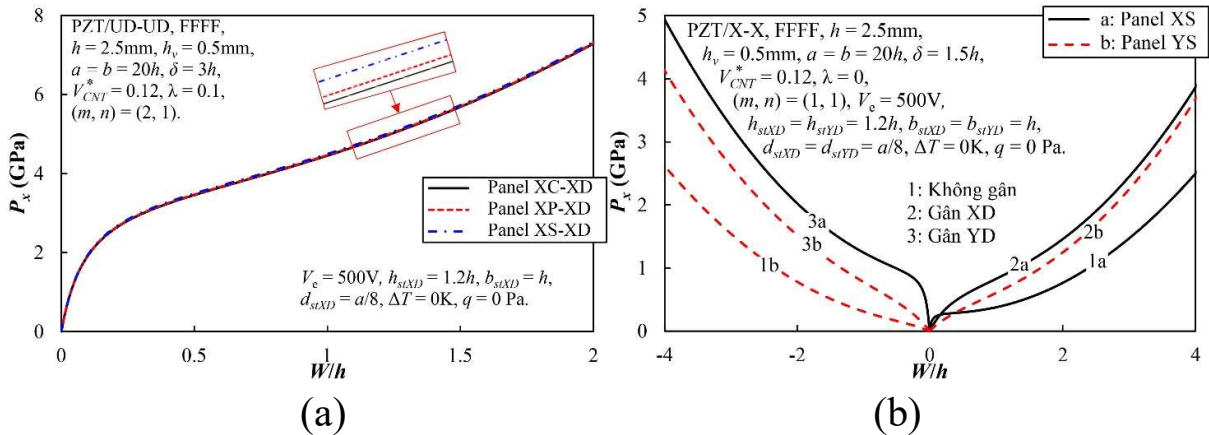


Fig. 3.5. Effects of panel type, stiffener orientation, distribution law and CNT volume fraction, geometrical rise and environment temperature on the static postbuckling curve of the axially compressed panel

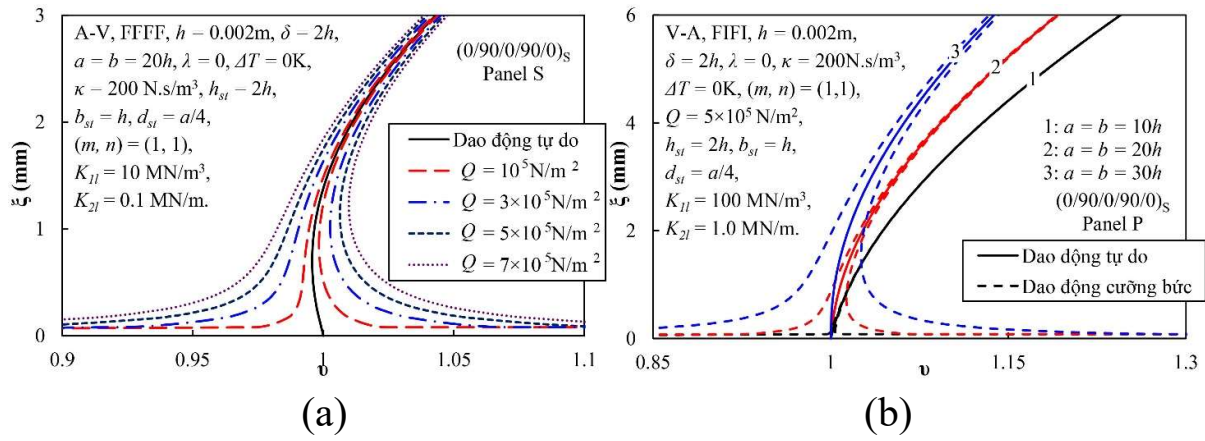


Fig. 3.11. Amplitude-frequency curves of free and forced vibrations of cylindrical, parabolic and sine panels with and without stiffeners

Table 3.5. Fundamental frequency (rad/s) of $(0)_{10T}$ cylindrical, parabolic and sine panels with and without stiffener (FFFF, $h=0.002\text{m}$, $a=b=20h$, $\delta=2h$, $\lambda=0$, $\Delta T=100\text{K}$, $m=n=1$, $h_{st}=2h$, $b_{st}=h$, $d_{st}=a/4=K_1=10\text{ MN/m}^3$, $K_2=0.1\text{ MN/m}$)

		Without stiffener	X stiffeners	Y stiffeners	X and Y stiffeners
UD-UD	Sine panel	83806.13	108887.78	108581.22	132787.50
	Parabolic panel	83470.90	108642.34	108330.80	132604.56
	Cylindrical panel	83458.89	108634.54	108321.98	132599.03
X-X	Sine panel	84913.92	108742.91	107992.01	131078.44
	Parabolic panel	84598.88	108509.79	107752.47	130903.04
	Cylindrical panel	84587.49	108502.28	107743.94	130897.65
V-A	Sine panel	79476.65	109680.63	108732.40	137252.32
	Parabolic panel	79141.97	109457.17	108503.33	137098.93
	Cylindrical panel	79129.88	109450.06	108495.25	137094.41
A-V	Sine panel	80162.03	97257.90	96694.17	113898.69
	Parabolic panel	79826.27	96988.88	96417.01	113680.54
	Cylindrical panel	79814.11	96980.11	96407.06	113673.62
O-O	Sine panel	77780.42	100846.02	100102.91	122707.17
	Parabolic panel	77436.37	100594.87	99844.74	122520.36
	Cylindrical panel	77423.93	100586.78	99835.55	122514.63

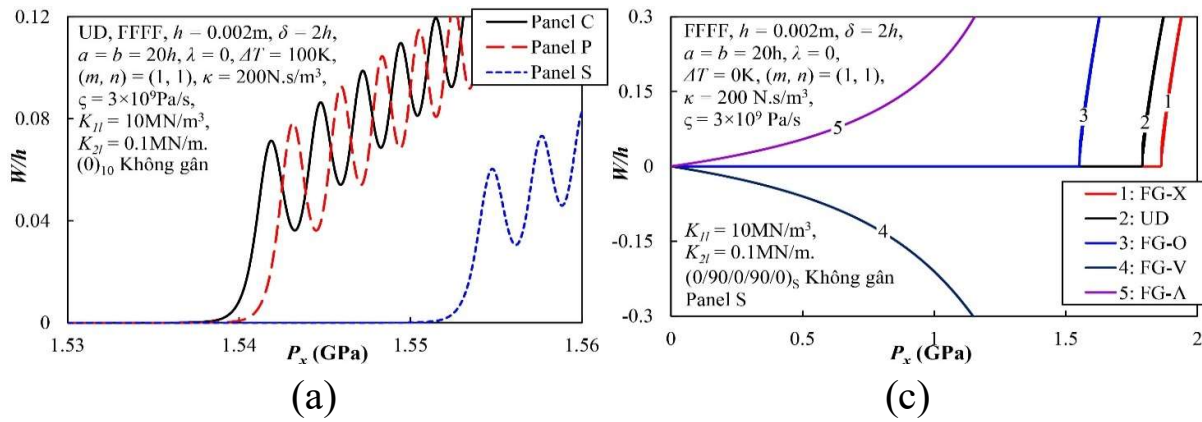


Fig. 3.13. Dynamic instability of cylindrical panels, parabolic panels and sine panels with and without stiffeners

3.5. Conclusion of Chapter 3

Some important comments are as follows

- The natural frequency, load-bearing capacity of stiffened panels are larger than that of unstiffened panels. The amplitude of stiffened panels is significantly smaller than that of unstiffened panels.

- Load-bearing capacity of the sine panel is larger than that of parabolic and cylindrical panels, although not significantly. Similarly, the sine panel has a slightly smaller amplitude than other panel types.

- The critical dynamic instability load and the dynamic instability phenomenon of the panel under axial compressive load can only be clearly observed for unstiffened panel with symmetrical distribution.

- Other geometrical and material parameters also significantly affect the stability and dynamic behavior of the panel.

CHAPTER 4: NONLINEAR STATIC STABILITY OF FG-GPLRC AND POROUS FG-GPLRC CYLINDRICAL SHELLS WITH ORTHOGONAL AND SPIRAL STIFFENERS

This chapter has applied Donnell shell theory and nonlinear theory to establish the basic equations. Ritz energy method is used to analyze the postbuckling curves and determine the critical buckling load.

4.1. Structural and material models

4.1.1. Model 1: Porous FG-GPLRC cylindrical shell with orthogonal stiffeners

The stiffened cylindrical shell is subjected to external pressure q .

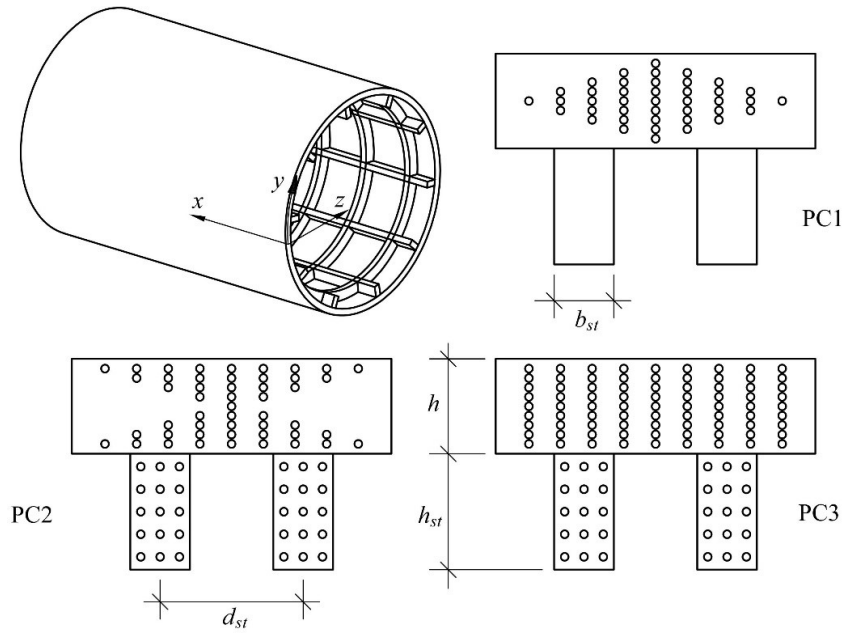


Fig. 4.1. Model and geometric parameters of orthogonally stiffened porous FG-GPLRC cylindrical shell

Three types of porosity distributions (PC1, PC2 and PC3) are considered in this chapter and the elastic modulus of the shell is expressed

$$\bar{E}_{sh} = \begin{cases} E_1 [1 - e_1 \cos(\pi z/h)], & \text{PC1} \\ E_1 \{1 - e_2 [1 - \cos(\pi z/h)]\}, & \text{PC2} \\ E_1 e_3, & \text{PC3} \end{cases} \quad (4.5)$$

and for the stiffeners

$$\bar{E}_{st} = \begin{cases} E_m, & \text{PC1} \\ E_m (1 - e_2), & \text{PC2} \\ E_m e_3, & \text{PC3} \end{cases} \quad (4.7)$$

in which e_1 , e_2 , and e_3 are the porosity ratios.

4.1.3. Model 2: FG-GPLRC cylindrical shell with spiral FG-GPLRC stiffeners

The five distributions of GPL are UD, FG-X, FG-O, FG-V and FG- Λ distributions for the shell and stiffeners are written similarly to chapter 2 when given as $h_v = 0$, specifically as follows

- UD-UD distribution (UD shell with UD stiffeners)

$$\Lambda_G^{sh} = \Lambda_G, \text{ for the shell,} \quad (4.9)$$

$$\Lambda_G^{st} = \Lambda_G, \text{ for stiffeners,} \quad (4.10)$$

X-X distribution (FG-X shell with FG-X stiffeners)

$$\Lambda_G^{sh} = 4|z|\Lambda_G/h, \text{ for the shell,} \quad (4.11)$$

$$\Lambda_G^{st} = \left[\frac{(2h-4z)}{h_{st}} + 2 \right] \Lambda_G, \text{ for stiffeners,} \quad (4.12)$$

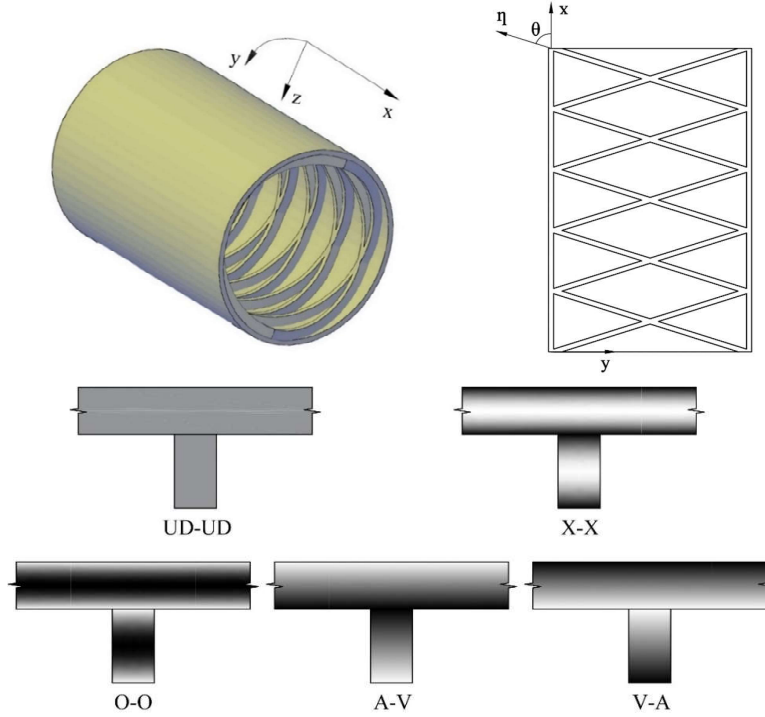


Fig. 4.2. Configuration, coordinate system and material distribution of FG-GPLRC cylindrical shell and spiral FG-GPLRC stiffeners

O-O distribution (FG-O shell with FG-O stiffeners)

$$\Lambda_G^{sh} = (1 - 2z/h)\Lambda_G, \text{ for the shell,} \quad (4.13)$$

$$\Lambda_G^{st} = \left[2 - \frac{(4z-2h)}{h_{st}} - 2 \right] \Lambda_G, \text{ for stiffeners,} \quad (4.14)$$

V-A distribution (FG-V shell with FG-A stiffeners)

$$\Lambda_G^{sh} = (1 - 2z/h)\Lambda_G, \text{ for the shell,} \quad (4.15)$$

$$\Lambda_G^{st} = \left[\frac{(2z-h)}{h_{st}} \right] \Lambda_G, \text{ for stiffeners,} \quad (4.16)$$

A-V distribution (FG-A sheath with FG-V stiffeners)

$$\Lambda_G^{sh} = (1 + 2z/h)\Lambda_G, \text{ for the shell,} \quad (4.17)$$

$$\Lambda_G^{st} = \left[2 + \frac{(h-2z)}{h_{st}} \right] \Lambda_G, \text{ for stiffeners,} \quad (4.18)$$

4.2. Governing equation system

The internal force of the shell has the form

$$\begin{bmatrix} N_x \\ N_y \\ N_{xy} \\ M_x \\ M_y \\ M_{xy} \end{bmatrix} = \begin{bmatrix} D_{11} & D_{12} & 0 & C_{11} & C_{12} & 0 \\ D_{12} & D_{22} & 0 & C_{12} & C_{22} & 0 \\ 0 & 0 & D_{66} & 0 & 0 & C_{66} \\ C_{11} & C_{12} & 0 & B_{11} & B_{12} & 0 \\ C_{12} & C_{22} & 0 & B_{12} & B_{22} & 0 \\ 0 & 0 & C_{66} & 0 & 0 & B_{66} \end{bmatrix} \begin{bmatrix} \varepsilon_x^0 \\ \varepsilon_y^0 \\ \gamma_{xy}^0 \\ -w_{,xx} \\ -w_{,yy} \\ -2w_{,xy} \end{bmatrix}, \quad (4.23)$$

Orthogonal stiffeners can be achieved by using the smeared stiffener technique for the FG-GPLRC stiffener, by

$$\begin{aligned} D_{11}^{st-ort} &= \frac{b_{stXD}}{d_{stXD}} E_1^{stXD}, D_{22}^{st-ort} = \frac{b_{stYD}}{d_{stYD}} E_1^{stYD}, D_{12}^{st-ort} = 0, D_{66}^{st-ort} = 0, \\ C_{11}^{st-ort} &= \frac{b_{stXD}}{d_{stXD}} E_2^{stXD}, C_{22}^{st-ort} = \frac{b_{stYD}}{d_{stYD}} E_2^{stYD}, C_{12}^{st-ort} = 0, C_{66}^{st-ort} = 0, \\ B_{11}^{st-ort} &= \frac{b_{stXD}}{d_{stXD}} E_3^{stXD}, B_{22}^{st-ort} = \frac{b_{stYD}}{d_{stYD}} E_3^{stYD}, B_{12}^{st-ort} = 0, B_{66}^{st-ort} = 0, \end{aligned} \quad (4.26)$$

Combining the coordinate system transformation technique with the FG-GPLRC smeared stiffener technique, lead to

$$\begin{aligned} D_{11}^{st-spr} &= 2 \frac{b_{stSPR}}{d_{stSPR}} E_1^{st-spr} \cos^4 \theta, D_{66}^{st-spr} = 2 \frac{b_{stSPR}}{d_{stSPR}} E_1^{st-spr} \sin^2 \theta \cos^2 \theta, \\ D_{12}^{st-spr} &= 2 \frac{b_{stSPR}}{d_{stSPR}} E_1^{st-spr} \sin^2 \theta \cos^2 \theta, D_{22}^{st-spr} = 2 \frac{b_{stSPR}}{d_{stSPR}} E_1^{st-spr} \sin^4 \theta, \\ C_{11}^{st-spr} &= 2 \frac{b_{stSPR}}{d_{stSPR}} E_2^{st-spr} \cos^4 \theta, C_{66}^{st-spr} = 2 \frac{b_{stSPR}}{d_{stSPR}} E_2^{st-spr} \sin^2 \theta \cos^2 \theta, \\ C_{12}^{st-spr} &= 2 \frac{b_{stSPR}}{d_{stSPR}} E_2^{st-spr} \sin^2 \theta \cos^2 \theta, C_{22}^{st-spr} = 2 \frac{b_{stSPR}}{d_{stSPR}} E_2^{st-spr} \sin^4 \theta, \\ B_{11}^{st-spr} &= 2 \frac{b_{stSPR}}{d_{stSPR}} E_3^{st-spr} \cos^4 \theta, B_{66}^{st-spr} = 2 \frac{b_{stSPR}}{d_{stSPR}} E_3^{st-spr} \sin^2 \theta \cos^2 \theta, \\ B_{12}^{st-spr} &= 2 \frac{b_{stSPR}}{d_{stSPR}} E_3^{st-spr} \sin^2 \theta \cos^2 \theta, B_{22}^{st-spr} = 2 \frac{b_{stSPR}}{d_{stSPR}} E_3^{st-spr} \sin^4 \theta, \end{aligned} \quad (4.27)$$

4.3. Boundary conditions and stress functions

The popular deflection form of the cylindrical shell is [4]

$$w(x,y) = f_0 + f_1 \sin \frac{m\pi x}{L} \sin \frac{ny}{R} + f_2 \sin^2 \frac{m\pi x}{L}, \quad (4.32)$$

4.4. Ritz energy method

For cylindrical shells, the closed condition must be satisfied, as

$$\int_0^{2\pi R} \int_0^L v_{,y} dx dy = \int_0^{2\pi R} \int_0^L \left(\varepsilon_y^0 + \frac{w}{R} - \frac{1}{2} w_{,y}^2 \right) dx dy = 0. \quad (4.34)$$

The total potential energy of the shell can be determined by

$$\Phi = - \int_0^L \int_0^{2\pi R} q w dx dy + \frac{1}{2} \int_{-\frac{h}{2}}^{\frac{h}{2}} \int_0^{2\pi R} \int_0^L \left(\varepsilon_x \sigma_x + \varepsilon_y \sigma_y + \gamma_{xy} \tau_{xy} \right) dx dy dz. \quad (4.36)$$

Apply the Ritz method, as follows

$$\frac{\partial \Phi}{\partial f_0} = \frac{\partial \Phi}{\partial f_1} = \frac{\partial \Phi}{\partial f_2} = 0. \quad (4.37)$$

Combining Eq. (4.37) with the closed condition (4.35), leads to

$$\lambda_{11} f_0 + \lambda_{12} f_1^2 + \lambda_{13} f_2 - 2q_0 = 0, \quad (4.38)$$

$$\lambda_{21} f_0 + \lambda_{22} f_1^2 + \lambda_{23} f_2^2 + \lambda_{24} f_2 + \lambda_{26} = 0, \quad (4.39)$$

$$\lambda_{31} f_0 + \lambda_{32} f_1^2 + \lambda_{33} f_1^2 f_2 + \lambda_{34} f_2 - q = 0, \quad (4.40)$$

The maximum deflection is in terms of amplitude f_2 , as follows

$$\begin{aligned} W_{max} = f_0 + f_1 + f_2 = & \frac{\lambda_{12} \lambda_{23}}{\lambda_{11} \lambda_{22} - \lambda_{12} \lambda_{21}} f_2^2 + \frac{\lambda_{12} \lambda_{24} - \lambda_{13} \lambda_{22}}{\lambda_{11} \lambda_{22} - \lambda_{12} \lambda_{21}} f_2 \\ & + \frac{2\lambda_{22}}{\lambda_{11} \lambda_{22} - \lambda_{12} \lambda_{21}} q + \frac{\lambda_{12} \lambda_{26}}{\lambda_{11} \lambda_{22} - \lambda_{12} \lambda_{21}} + \left[-\frac{\lambda_{23} \lambda_{11}}{\lambda_{11} \lambda_{22} - \lambda_{12} \lambda_{21}} f_2^2 \right. \\ & \left. - \frac{\lambda_{11} \lambda_{24} - \lambda_{13} \lambda_{21}}{\lambda_{11} \lambda_{22} - \lambda_{12} \lambda_{21}} f_2 - \frac{2\lambda_{21}}{\lambda_{11} \lambda_{22} - \lambda_{12} \lambda_{21}} q - \frac{\lambda_{11} \lambda_{26}}{\lambda_{11} \lambda_{22} - \lambda_{12} \lambda_{21}} \right]^{\frac{1}{2}} + f_2. \end{aligned} \quad (4.41)$$

Amplitude f_0 and f_2 obtained from Eqs. (4.38) and (4.40), then substituting these amplitudes into expression (4.39), lead to

$$q = - \frac{\delta_{11} f_2^3 + \delta_{12} f_2^2 + \delta_{13} f_2 + \delta_{18}}{\delta_{15} f_2 + \delta_{17}}, \quad (4.42)$$

The postbuckling curve $W_{max} - q$ is determined by combining the relations $W_{max} - f_2$ and $q_0 - f_2$.

4.5. Numerical results and discussions

Table 4.3. Critical buckling load of stiffened porous FG-GPLRC cylindrical shells with different porosity distributions and ratios (MPa, $L/R=1.5$, $R/h=100$, $h=0.04\text{m}$, $W_{GPL}=0.6\%$, $h_{stXD}=h_{stYD}=1.5h$, $b_{stXD}=b_{stYD}=h$, $d_{stXD}=d_{stYD}=5h$)

	e_1	0	0.1	0.2	0.3	0.5
Without stiffener	PC1	1.178(1.7)	1.129(1.7)	1.080(1.7)	1.030(1.7)	0.932(1.7)
	PC2	1.178(1.7)	1.059(1.7)	0.942(1.7)	0.828(1.7)	0.613(1.7)
	PC3	1.178(1.7)	1.103(1.7)	1.027(1.7)	0.950(1.7)	0.793(1.7)
Orthogonal stiffener	PC1	3.779(1.6)	3.687(1.6)	3.592(1.6)	3.477(1.5)	3.174(1.5)
	PC2	3.779(1.6)	3.275(1.6)	2.769(1.6)	2.262(1.6)	1.251(1.6)
	PC3	3.779(1.6)	3.538(1.6)	3.294(1.6)	3.048(1.6)	2.544(1.6)

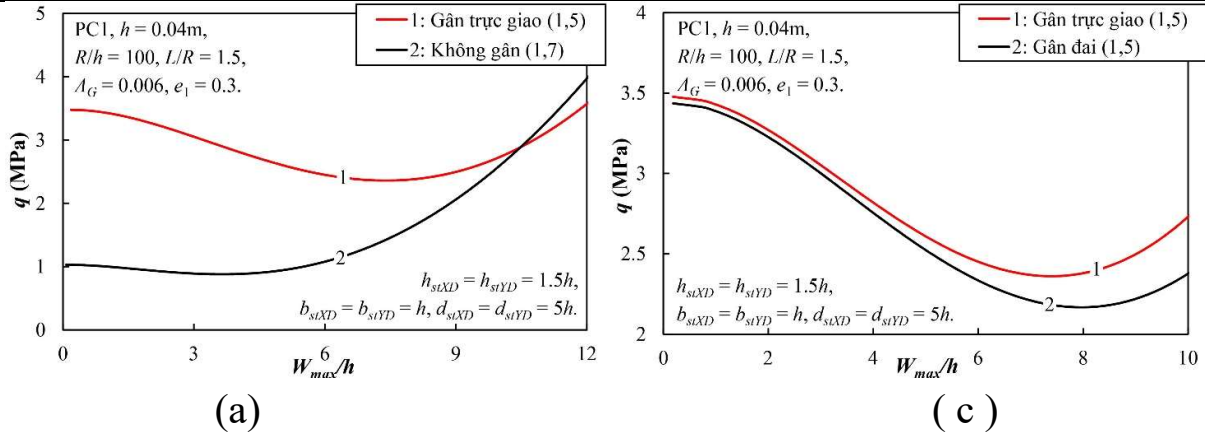


Fig. 4.3. Effect of porous FG-GPLRC stiffeners on the postbuckling response of porous FG-GPLRC cylindrical shells

Table 4.4. Critical buckling load of FG-GPLRC cylindrical shell without stiffeners, with orthogonal stiffeners and spiral stiffeners

	Without stiffener	Orthogonal stiffener	Spiral stiffener
UD-UD	2.0504(1,7)	11.6329(1,5)	15.6318(1,4,42,70.47)*
X-X	2.1871(1,6)	11.8650(1,5)	15.8350(1,4,42,70.47)
A-V	2.0218(1,7)	10.6680(1,5)	14.3298(1,5,42,70.47)
V-A	2.0115(1,7)	12.5163(1,5)	16.4522(1,4,42,70.47)
O-O	1.8645(1,7)	11.3340(1,5)	15.2994(1,5,42,70.47)

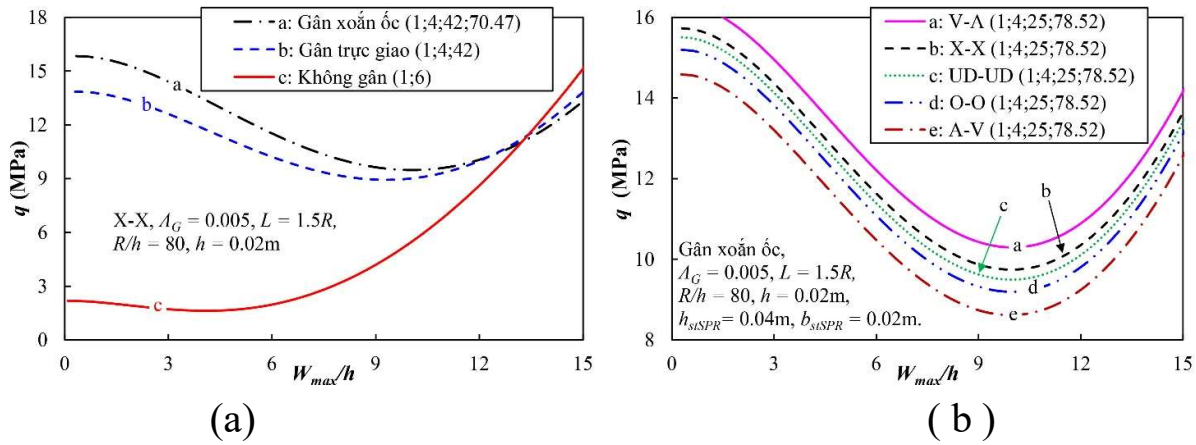


Fig. 4.5. Effect of stiffener type and material parameters on the postbuckling response of FG-GPLRC cylindrical shell

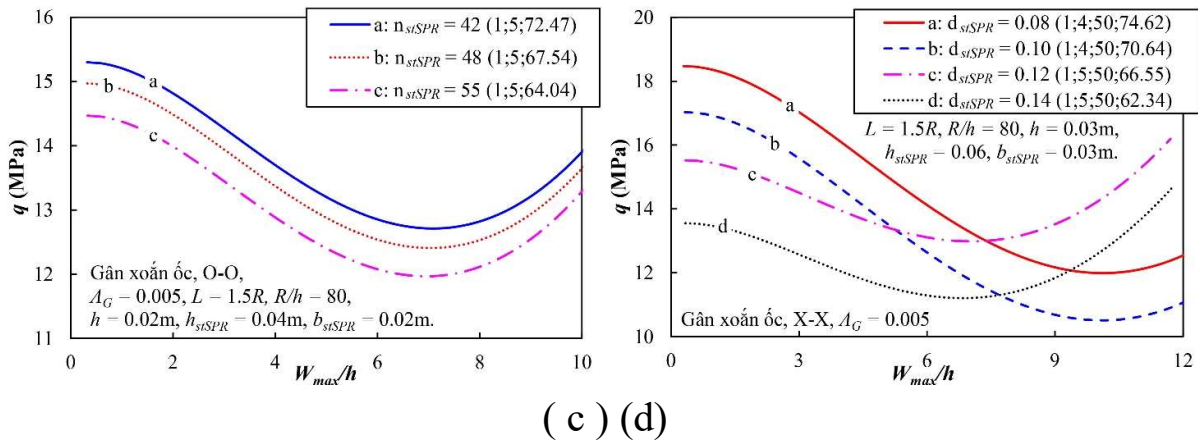


Fig. 4.6. Effect of geometric parameters of shell and stiffeners on the postbuckling response of FG-GPLRC cylindrical shell

4.6. Conclusion of chapter 4

Some of the observations that can be made are as follows:

- 1) The stiffeners have a large influence on the critical load and postbuckling behavior. The effect of spiral stiffeners is significantly greater than that of the corresponding orthogonal stiffeners.
- 2) Snap-through phenomenon can be clearly observed in orthogonally stiffened and spirally stiffened cases, and is more difficult to observe in unstiffened cases and is most evident in the spirally stiffened case.
- 3) Effects of geometry, material properties, porosity ratio, porosity distribution and GPL mass fraction on the critical buckling load and postbuckling curves of FG-GPLRC and stiffened porous FG-GPLRC cylindrical shells can be observed.

CONCLUSIONS

The thesis has obtained the following new results:

1. Proposed stiffener design and developed an improved smeared stiffener technique for the FG-GPLRC and porous cored FG-GPLRC circular plates and spherical shells with two- and three-region spiderweb stiffeners. Developed analytical and semi-analytical solutions based on Donnell shell theory and energy method for the stability and nonlinear dynamics of structures subjected to mechanical and thermal loads.

2. Proposed stiffener design and establish solution for panels with complex curvature, including cylindrical, parabolic and sine panels made of FG-CNTRC and FG-GRC by orthogonal FG-CNTRC and FG-GRC stiffeners respectively, according to HSDT and energy method.

3. Proposed stiffening method and built solution for porous FG-GPLRC and FG-GPLRC cylindrical shell structure by orthogonal and spiral stiffeners system of porous FG-GPLRC and FG-GPLRC respectively according to Donnell shell theory and energy method.

4. Applied the results of analytical and semi-analytical approaches to analyze in detail the effects of stiffeners in the corresponding problems, elastic foundation, imperfections of circular plates and spherical shells FG-GPLRC, and panels with complex curvatures FG-CNTRC and FG-GRC, geometric dimensions,... on the static, dynamic stability and nonlinear vibration behavior of plates and shells.

RECOMMENDATIONS FOR FURTHER RESEARCH

1. Study on stability and nonlinear dynamics of stiffened nanocomposite spherical shell and circular plate based on shear deformation theories.

2. Study on stability and nonlinear dynamics of stiffened nanocomposite shells with complex curvature in two directions.

3. Study on stability and nonlinear dynamics of stiffened nanocomposite cylindrical shells and drum shells based on shear deformation theories.

4. Study on stability and nonlinear dynamics of stiffened nanocomposite plates and shells subjected to complex loads.

5. Research and develop design standards for stiffened nanocomposite shell panels with stiffeners for construction works.

LIST OF AUTHOR'S SCIENTIFIC PUBLICATIONS RELATED TO THE THESIS

The thesis published 7 papers, including 3 ISI papers (SCIE):

1. V.H. Nam, T.Q. Minh, P.T. Hieu, V.T. Hung, B.T. Tu, N.T.T. Hoai, D.T. Dong, A new analytical approach for nonlinear thermo-mechanical postbuckling of FG-GPLRC circular plates and shallow spherical caps stiffened by spiderweb stiffeners, *Thin-Walled Struct.* 2023;193:111296. (SCIE, Q1)
2. T.Q. Minh, V.H. Nam, V.M. Duc, V.T. Hung, L.N. Ly, N.T. Phuong. Nonlinear vibration and dynamic buckling responses of stiffened functionally graded graphene-reinforced cylindrical, parabolic, and sinusoid panels using the higher-order shear deformation theory. *ZAMM J. Appl. Math. Mech.* 2024;104:e202300580. (SCIE, Q2)
3. V.M. Duc, T.Q. Minh, N.T. Phuong, V.T. Hung, V.H. Nam, Nonlinear dynamic responses of CNT-reinforced panels with complex curvature, piezoelectric layer, and CNT-reinforced stiffeners, *Eur. J. Mech. A/Solids* 2024;106:105341. (SCIE, Q1)
4. L.N. Quang, V.M. Duc, T.Q. Minh. Nonlinear buckling and postbuckling behaviors of porous FG-GPLRC cylindrical shells with stiffeners subjected to external pressure. *J. Sci. Transp. Technol.* 2024;4(2):24-36.
5. V.M. Duc, T.Q. Minh, D.T.K. My, C.V. Doan, N.V. Tien. Nonlinear buckling analysis of spirally stiffened functionally graded graphene platelet reinforced cylindrical shells subjected to external pressure. *Proceeding of national conference on mechanics, Hanoi, 2024.* 130-140.
6. D.T. Dong, C.V. Doan, V.T. Hung, T.Q. Minh. Nonlinear buckling of the FG-GPLRC cylindrical and half-sinusoid panels reinforced by orthogonal stiffeners under axial compression load. *Proceeding of national conference on mechanics, Hanoi, 2024.* 186-195.
7. T.Q. Minh, V.M. Duc, D.T. Dong, V.H. Nam. Nonlinear buckling analysis of higher-order shear deformable FG-CNTRC plates stiffened by oblique FG-CNTRC stiffeners. *Vietnam Journal of Mechanics* 2022;44(4):431–444.